Two New Noncentrosymmetric Polar Oxides: Synthesis, Characterization, Second-Harmonic Generating, and Pyroelectric Measurements on $TlSeVO_5$ and $TlTeVO_5$

T. Sivakumar, Hong Young Chang, Jaewook Baek, and P. Shiv Halasyamani*

Department of Chemistry and Center for Materials Chemistry, University of Houston, 136 Fleming Building, Houston, Texas 77204-5003

Received May 2, 2007. Revised Manuscript Received July 11, 2007

Two new noncentrosymmetric (NCS) polar quaternary oxides, $TlMVO_5$ ($M = Se^{4+}$ or Te^{4+}), have been synthesized by hydrothermal techniques using Tl_2CO_3, SeO_2 (TeO_2), and V_2O_5 as reagents. The structures were determined by single-crystal X-ray diffraction ($TlSeVO_5$, orthorhombic, space group $Pna2_1$ (No. 33) with $a = 7.1639(15)$ Å, $b = 8.6630(19)$ Å, $c = 7.8946(17)$ Å, $V = 489.95(18)$ Å^3, and $Z = 4$; $TlTeVO_5$, orthorhombic, space group $Pna2_1$ (No. 33) with $a = 7.319(3)$ Å, $b = 8.749(4)$ Å, $c = 7.868(3)$ Å, $V = 503.8(4)$ Å^3, $Z = 4$). The materials exhibit NCS and polar three-dimensional structures consisting of chains of corner shared VO_6 octahedra connected by SeO_3 (TeO_4) and TlO_8 polyhedra. The V^{5+}, Se^{4+} (Te^{4+}), and Tl^+ cations are in asymmetric coordination environments attributable to second-order Jahn−Teller (SOJT) effects. The V^{5+} cations undergo intra-octahedral distortions toward an edge (local C_2 direction), whereas the Se^{4+} (Te^{4+}) and Tl^+ cations are in distorted coordination environments attributable to their lone-pair. As the materials are NCS and polar, second-harmonic generating (SHG), ferroelectric, and pyroelectric measurements were performed. The SHG measurements, using 1064 nm radiation, revealed doubling efficiencies of ~40 × α-SiO_2 for both $TlSeVO_5$ and $TlTeVO_5$. Ferroelectric measurements indicated the materials are not "switchable"; that is, the local dipole moment cannot be reversed in the presence of an external electric field. Pyroelectric measurements revealed a total pyroelectric coefficient, p, of −2.9 and −1.9 $\mu C/m^2 \cdot K$, for $TlSeVO_5$ and $TlTeVO_5$, respectively. Infrared, Raman, UV−vis diffuse reflectance spectroscopy, and thermal analyses are also presented.

Introduction

Noncentrosymmetric (NCS) compounds are of current interest in materials chemistry due to their technologically important properties such as second-harmonic generation (SHG), piezoelectricity, ferroelectricity, and pyroelectricity.[1−4] With inorganic materials, the macroscopic acentricity is often a manifestation of the asymmetric coordination environments of the metal cations. The asymmetry is a necessary but not sufficient condition for producing crystallographic NCS. That is, the material may crystallize with the asymmetric units aligned in an inversion relationship, leading to overall crystallographic centrosymmetry. Recently, a variety of strategies have been put forth for the design of new NCS materials.[5−10] We have focused on creating new NCS materials[11−16] by synthesizing oxides containing cations susceptible to second-order Jahn−Teller (SOJT) distortions.[17−23] The distortion can occur in two different types of cations, d^0 transition metals (Ti^{4+}, V^{5+}, Nb^{5+}, Mo^{6+}, W^{6+}) and cations with stereoactive lone-pairs (Se^{4+}, Te^{4+}, Sb^{3+}, Bi^{3+}, Pb^{2+}, Sn^{2+}, Tl^+), and results in asymmetric coordination environments.

We have chosen to investigate the Tl^+−Se^{4+} (Te^{4+})−d^0−oxide system, especially, where not only the d^0 transition

* To whom correspondence should be addressed. Phone: (713) 743-3278. Fax: (713) 743-0796. E-mail: psh@uh.edu.

(1) Nye, J. *Physical Properties of Crystals*; Oxford University Press: Oxford, 1957.
(2) Cady, W. G. *Piezoelectricity; an Introduction to the Theory and Applications of Electromechanical Phenomena in Crystals*; Dover: New York, 1964.
(3) Jona, F.; Shirane, G. *Ferroelectric Crystals*; Pergamon Press: Oxford, 1962.
(4) Lang, S. B. *Sourcebook of Pyroelectricity*; Gordon & Breach: London, 1974.
(5) Bruce, D.; Wilkinson, A. P.; While, M. G.; Bertrand, J. A. *J. Solid State Chem.* **1996**, *125*, 228.
(6) Kepert, C. J.; Prior, T. J.; Rosseinsky, M. J. *J. Am. Chem. Soc.* **2000**, *122*, 5158.
(7) Maggard, P. A.; Stern, C. L.; Poeppelmeier, K. R. *J. Am. Chem. Soc.* **2001**, *123*, 7742.
(8) Welk, M. E.; Norquist, A. J.; Arnold, F. P.; Stern, C. L.; Poeppelmeier, K. R. *Inorg. Chem.* **2002**, *41*, 5119.
(9) Evans, O. R.; Lin, W. *Acc. Chem. Res.* **2002**, *35*, 511.
(10) Hwu, S.-J.; Ulutagay-Kartin, M.; Clayhold, J. A.; Mackay, R.; Wardojo, T. A.; O'Connor, C. J.; Kraweic, M. *J. Am. Chem. Soc.* **2002**, *124*, 12404.
(11) Halasyamani, P. S.; Poeppelmeier, K. R. *Chem. Mater.* **1998**, *10*, 2753.
(12) Porter, Y.; Ok, K. M.; Bhuvanesh, N. S. P.; Halasyamani, P. S. *Chem. Mater.* **2001**, *13*, 1910.
(13) Goodey, J.; Broussard, J.; Halasyamani, P. S. *Chem. Mater.* **2002**, *14*, 3174.
(14) Ra, H.-S.; Ok, K. M.; Halasyamani, P. S. *J. Am. Chem. Soc.* **2003**, *125*, 7764.
(15) Goodey, J.; Ok, K. M.; Broussard, J.; Hofmann, C.; Escobedo, F. V.; Halasyamani, P. S. *J. Solid State Chem.* **2003**, *175*, 3.
(16) Chi, E. O.; Ok, K. M.; Porter, Y.; Halasyamani, P. S. *Chem. Mater.* **2006**, *18*, 2070.
(17) Opik, U.; Pryce, M. H. L. *Proc. R. Soc. London* **1957**, *A238*, 425.
(18) Bader, R. F. W. *Mol. Phys.* **1960**, *3*, 137.
(19) Bader, R. F. W. *Can. J. Chem.* **1962**, *40*, 1164.
(20) Pearson, R. G. *J. Am. Chem. Soc.* **1969**, *91*, 4947.
(21) Pearson, R. G. *J. Mol. Struct. (THEOCHEM)* **1983**, *103*, 25.
(22) Wheeler, R. A.; Whangbo, M.-H.; Hughbanks, T.; Hoffmann, R.; Burdett, J. K.; Albright, T. A. *J. Am. Chem. Soc.* **1986**, *108*, 2222.
(23) Kunz, M.; Brown, I. D. *J. Solid State Chem.* **1995**, *115*, 395.

10.1021/cm071188p CCC: $37.00
Published on Web 08/21/2007

metal is V^{5+} (strong distorter),[24,25] but also to couple the SOJT distortions of d^0 (V^{5+}) cation with two different lone-pair cations (Se^{4+} or Te^{4+} and Tl^+) and thereby promote the formation of new NCS materials. With respect to oxides containing octahedrally coordinated d^0 cation with two different lone-pair cations, a few compounds, $BiTe_2NbO_8$,[26] $Pb_4Te_6M_{10}O_{41}$ (M = Nb or Ta),[27] $Bi_2Te_2WO_{10}$,[28] $Bi_2Te_2W_3O_{16}$,[29] $Tl_2(MoO_3)_3SeO_3$,[30] and $Tl_2TeMo_2O_6(PO_4)_2$,[31] have been reported. Among these compounds, $Tl_2(MoO_3)_3SeO_3$[30] is noncentrosymmetric. Our investigation of the Tl−Se(Te)−V−oxide system resulted in the synthesis of two new noncentrosymmetric materials, $TlSeVO_5$ and $TlTeVO_5$. The syntheses, structures, and characterization of these two materials are reported.

Experimental Section

Reagents. Tl_2CO_3 (Alfa Aesar, 99%), SeO_2 (Alfa Aesar, 99.4%), TeO_2 (Aldrich, 99+%), and V_2O_5 (Aldrich, 99.6+%) were used as received.

Syntheses. For $TlSeVO_5$, 0.4568 g (1 mmol) of Tl_2CO_3, 0.6103 g (5.5 mmol) of SeO_2, and 0.1818 g (1 mmol) of V_2O_5 were combined with 10 mL of H_2O. For $TlTeVO_5$, 0.2284 g (0.5 mmol) of Tl_2CO_3, 0.1595 g (1 mmol) of TeO_2, and 0.0909 g (0.5 mmol) of V_2O_5 were combined with 10 mL of H_2O. The respective solutions were placed in 23-mL Teflon-lined autoclaves that were subsequently sealed. The autoclaves were gradually heated to 230 °C, held for 3 d, and cooled slowly to room temperature at a rate of 6 °C h^{-1}. The mother liquor was decanted from the products, and the products were recovered by filtration and washed with distilled water. Yellow crystals, the only product from each reaction, were obtained in near quantitative yield.

Single-Crystal X-ray Diffraction. For $TlSeVO_5$ and $TlTeVO_5$, yellow blocks 0.07 × 0.04 × 0.02 mm^3 and 0.06 × 0.03 × 0.02 mm^3, respectively, were used for single-crystal data analyses. Data were collected using a Siemens SMART diffractometer equipped with a 1K CCD area detector using graphite monochromated Mo Kα radiation. A hemisphere of data was collected using a narrow-frame method with scan widths of 0.30 in., and an exposure time of 25 s per frame. The first 50 frames were remeasured at the end of the data collection to monitor instrument and crystal stability. The maximum correction applied to the intensities was <1%. The data were integrated using the Siemens SAINT program,[32] with the intensities corrected for Lorentz polarization, air absorption, and absorption attributable to the variation in the path length through the detector faceplate. Ψ-scans were used for the absorption correction on the hemisphere of data. The data were solved by direct methods using SHELXS-97[33] and refined using SHELXL-97.[34] All atoms were refined with anisotropic thermal parameters. The refinement converged for $I > 2\sigma(I)$. All calculations were performed using the WinGX-98 crystallographic software package.[35] Relevant crystallographic data, atomic coordinates, and selected bond distances are given in Tables 1−5.

Table 1. Crystallographic Data for $TlMVO_5$ (M = Se, Te)

formula	$TlSeVO_5$	$TlTeVO_5$
fw	414.27	462.91
space group	$Pna2_1$ (No. 33)	$Pna2_1$ (No. 33)
a (Å)	7.1639(15)	7.319(3)
b (Å)	8.6630(19)	8.749(4)
c (Å)	7.8946(17)	7.868(3)
α (deg)	90	90
β (deg)	90	90
γ (deg)	90	90
V (Å^3)	489.95(18)	503.8(4)
Z	4	4
T (K)	293.0(2)	293.0(2)
λ (Å)	0.71073	0.71073
reflections collected	1196	1196
Flack parameter	−0.021(11)	−0.002(12)
ρ_{calcd} (g cm^{-3})	5.616	6.103
$R(F)^a$	0.0271	0.0442
$R_w(F_o^2)^b$	0.0606	0.1156

^{a} $R(F) = \sum||F_o| - |F_c||/\sum|F_o|$. ^{b} $R_w(F_o^2) = [\sum w(F_o^2 - F_c^2)^2/\sum w(F_o^2)^2]^{1/2}$.

Table 2. Atomic Coordinates for $TlSeVO_5$

atom	x	y	z	$U_{(eq)}$ (Å^2)^a
Tl	0.02531(5)	0.11711(4)	0.10075(7)	0.0258(2)
Se	−0.04792(11)	0.48408(9)	0.40380(10)	0.0066(2)
V	−0.2152(2)	0.2624(1)	0.6946(2)	0.0075(3)
O(1)	−0.2223(8)	0.1790(7)	0.5078(9)	0.0145(12)
O(2)	0.1087(9)	0.6271(6)	0.4303(7)	0.0086(11)
O(3)	−0.4329(8)	0.3239(6)	0.7282(7)	0.0091(11)
O(4)	−0.1083(8)	0.4575(6)	0.6142(8)	0.0109(10)
O(5)	−0.2491(8)	0.0800(7)	0.8422(8)	0.0131(12)

^{a} $U_{(eq)}$ is defined as one-third of the trace of the orthogonalized U_{ij} tensor.

Powder X-ray Diffraction. Powder X-ray diffraction (XRD) was used to confirm the phase purity of each sample. The powder XRD data were collected on a Scintag XDS2000 diffractometer at room temperature (Cu Kα radiation, $\theta-\theta$ mode, flat plate geometry) equipped with Peltier germanium solid-state detector in the 2θ range 3−70° with a step size of 0.02. The experimental powder XRD data are in good agreement with the calculated data based on the single-crystal models (see Supporting Information, Figures S3 and S4).

Infrared and Raman Spectroscopy. Infrared spectra were recorded on a Matteson FTIR 5000 spectrometer in the 400−4000 cm^{-1} range, with the sample pressed between two KBr pellets. Raman spectra were recorded at room temperature under the control of a Spex DM3000 microcomputer system using a conventional scanning Raman instrument equipped with a Spex 1403 double monochromator (with a pair of 1800 grooves/mm gratings) and a Hamamatsu 928 photomultiplier detector. The powder samples were placed in separate capillary tubes during the experiment. Excitation was provided by a coherent Ar^+ ion laser at a wavelength of 457 nm with 100 mW laser power and 4 cm^{-1} slit widths.

UV−Vis Diffuse Reflectance Spectroscopy. UV−vis diffuse reflectance data for the title compounds were collected on a Varian Cary 500 scan UV−vis−NIR spectrophotometer over the spectral range 300−1500 nm at room temperature. Poly(tetrafluoroethylene) was used as a reference material. Reflectance spectra were converted to absorbance with the Kubelka−Munk function.[36]

(24) Halasyamani, P. S. *Chem. Mater.* **2004**, *16*, 3586.
(25) Ok, K. M.; Halasyamani, P. S.; Casanova, D.; Llunell, M.; Alemany, P.; Alvarez, S. *Chem. Mater.* **2006**, *18*, 3176.
(26) Blanchandin, S.; Champarnaud-Mesjard, J. C.; Thomas, P.; Frit, B. *Solid State Sci.* **2000**, *2*, 223.
(27) Ok, K. M.; Halasyamani, P. S. *Inorg. Chem.* **2004**, *43*, 4248.
(28) Champarnaud-Mesjard, J. C.; Frit, B.; Chagraoui, A.; Tairi, A. *Z. Anorg. Allg. Chem.* **1996**, *622*, 1907.
(29) Champarnaud-Mesjard, J. C.; Frit, B.; Chagraoui, A.; Tairi, A. *J. Solid State Chem.* **1996**, *127*, 248.
(30) Dussack, L. L.; Harrison, W. T. A.; Jacobson, A. J. *Mater. Res. Bull.* **1996**, *31*, 249.
(31) Guesdon, A.; Raveau, B. *Chem. Mater.* **2000**, *12*, 2239.
(32) *SAINT Version 4.05, Program for Area Detector Absorption Correction*; Siemens Analytical X-ray Instruments: Madison, WI, 1995.
(33) Sheldrick, G. M. *SHELXS-97-A program for automatic solution of crystal structures*; University of Goettingen: Goettingen, Germany, 1997.
(34) Sheldrick, G. M. *SHELXL-97-A program for crystal structure refinement*; University of Goettingen: Goettingen, Germany, 1997.
(35) Farrugia, L. J. *J. Appl. Crystallogr.* **1999**, *32*, 837.

Thermogravimetric Analysis. Thermogravimetric analyses were carried out on a TGA 2050 thermogravimetric analyzer (TA instruments). The sample was contained within a platinum crucible and heated in flowing nitrogen at a rate of 10 °C min^{-1} to 1000 °C.

Differential Scanning Calorimetry. Differential scanning calorimetric analyses were also carried out on a DSC 2920 differential scanning calorimeter (TA instruments). The sample was placed in an aluminum pan and heated in flowing nitrogen at a rate of 5 °C min^{-1} to a maximum of 500 °C.

Second Harmonic Generation. Powder SHG measurements were performed on a modified Kurtz-NLO system[37] using a pulsed Nd:YAG laser with a wavelength of 1064 nm. A detailed description of the equipment and methodology has been published.[12,38] Because the SHG efficiency has been shown to depend strongly on particle size, samples were ground and sieved into distinct particle size ranges (20−45, 45−63, 63−75, 75−90, >90 μm). To make relevant comparisons with known SHG materials, crystalline SiO_2 and $LiNbO_3$ were also ground and sieved into the same particle size ranges. No index matching fluid was used in any of the experiments.

Piezoelectric Measurements. Converse piezoelectric measurements were performed using a Radiant Technologies RT66A piezoelectric test system with a TREK (model 609E-6) high voltage amplifier, Precision Materials Analyzer, Precision High Voltage Interface, and MTI 2000 Fotonic Sensor.

Ferroelectric and Pyroelectric Measurements. Polarization measurements were carried out on a Radiant Technologies RT66A ferroelectric test system with a TREK high-voltage amplifier in a Delta 9023 environmental test chamber. The pyroelectric coefficient, defined as d*P*/d*T* (change in polarization with respect to the change in temperature), was determined by measuring the polarization as a function of temperature. A detailed description of the methodology used has been published elsewhere.[16] The samples were pressed into pellets (12 mm diameter, ∼1 mm thick) and sintered, well below the decomposition temperatures, at 230 and 300 °C for 12 h for $TlSeVO_5$ and $TlTeVO_5$, respectively. Conducting silver paste was applied to both sides of the pellet for electrode and cured at 200 °C for 3 h. The polarization was measured statically from room temperature to 85 °C in 15 °C increments, with an electric field of 20 kV/cm. The temperature was allowed to stabilize before the polarization was measured.

Results

Structures. *$TlSeVO_5$.* $TlSeVO_5$ is a new quaternary Tl^+−Se^{4+}−V^{5+}−oxide exhibiting a three-dimensional structure that consists of corner shared VO_6 octahedra connected by asymmetric SeO_3 and TlO_8 polyhedra (see Figure 1). The crystal structure of $TlSeVO_5$ may be thought of consisting of chains of corner shared VO_6 octahedra that run along the *a*-axis. Inter- and intrachain bonds are made by the SeO_3 polyhedra. The TlO_8 ploydedra are involved in connecting the VO_6 and SeO_3 groups, resulting in the three-dimensional structure (see Figure 1). Interestingly, each of the cations, V^{5+}, Se^{4+}, and Tl^+, are in asymmetric coordination environments attributable to SOJT effects. The V^{5+} cation is in a distorted octahedral environment bonded to six oxygen atoms, with V−O bond distances ranging from 1.643(7) to 2.227(5) Å. The V^{5+} cations undergo an out-of-center distortion attributable to SOJT effects that creates bond asymmetries within the VO_6 octahedron. Two "short" (1.643(7) and 1.669(6) Å), two "normal" (1.961(5) and 1.978(6) Å), and two "long" (2.172(6) and 2.227(5) Å) V−O bonds are observed, resulting in a V^{5+} distortion toward an edge of the VO_6 octahedron (local C_2 direction). The Se^{4+} cations are in distorted trigonal pyramidal environments, attributable to their lone-pair, bonded to three oxygen atoms. The Se−O bond distances range from 1.685(6) to 1.744(6) Å. The Tl^+ cations are also in asymmetric coordinate environments, attributable to their lone-pair, bonded to eight oxygen atoms. The Tl−O bond distances range from 2.764(5) to 3.294(6) Å (see Table 3). In connectivity terms, the structure may be written as $[(VO_{5/2}O)^{2-}(SeO_{3/2})^+]^-$ with charge balance maintained by the Tl^+ cation. The bond valence calculations[39,40] resulted in values of 1.02, 3.84, and 4.94 for Tl^+, Se^{4+}, and V^{5+} cations, respectively.

$TlTeVO_5$. Although $TlTeVO_5$ and $TlSeVO_5$ crystallize in the same space group, $Pna2_1$, and have similar unit cell parameters, the compounds are not iso-structural. $TlTeVO_5$ is a new quaternary Tl^+−Te^{4+}−V^{5+}−oxide that exhibits a three-dimensional crystal structure consisting of VO_6 octahedra and TeO_4 and TlO_8 polyhedra (see Figure 2). Similar

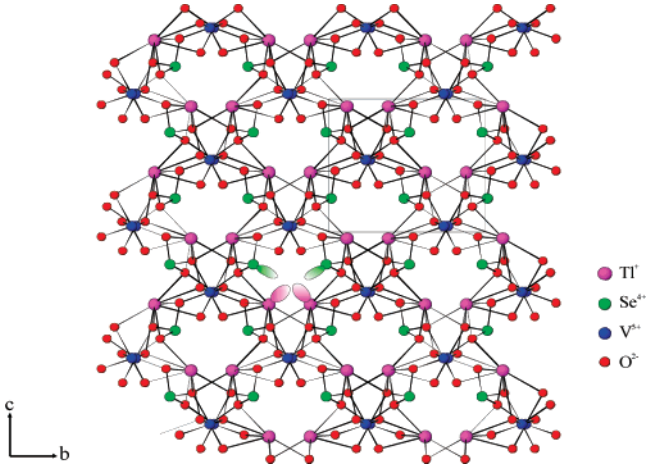

Figure 1. Ball-and-stick representation of $TlSeVO_5$ in the *bc*-plane is shown. The lone-pair on Tl^+ (purple) and Se^{4+} (green) are shown schematically and point toward the "gaps" in the structure.

Table 3. Selected Bond Distances (Å) for $TlSeVO_5$

	bond distance
V−O(1)	1.643(7)
V−O(2)	2.227(5)
V−O(3)	1.669(6)
V−O(3)	2.172(6)
V−O(4)	1.961(5)
V−O(5)	1.978(6)
Se−O(2)	1.685(6)
Se−O(4)	1.732(6)
Se−O(5)	1.744(6)
Tl−O(1)	3.018(6)
Tl−O(2)	2.764(5)
Tl−O(2)	2.948(6)
Tl−O(3)	2.811(5)
Tl−O(3)	3.000(6)
Tl−O(4)	3.294(6)
Tl−O(5)	2.852(6)
Tl−O(5)	3.019(6)

(36) Kubelka, P.; Munk, F. *Z. Tech. Phys.* **1931**, *12*, 593.
(37) Kurtz, S. K.; Perry, T. T. *J. Appl. Phys.* **1968**, *39*, 3798.
(38) Ok, K. M.; Bhuvanesh, N. S. P.; Halasyamani, P. S. *J. Solid State Chem.* **2001**, *161*, 57.
(39) Brown, I. D.; Altermatt, D. *Acta Crystallogr.* **1985**, *B41*, 244.
(40) Brese, N. E.; O'Keeffe, M. *Acta Crystallogr.* **1991**, *B47*, 192.

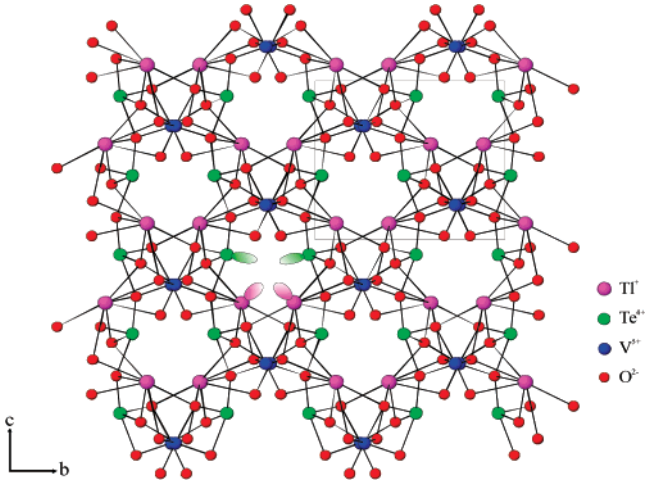

Figure 2. Ball-and-stick representation of $TlTeVO_5$ in the *bc*-plane is shown. The lone-pair on Tl^+ (purple) and Te^{4+} (green) are shown schematically and point toward the "gaps" in the structure.

Table 4. Atomic Coordinates for $TlTeVO_5$

atom	*x*	*y*	*z*	$U_{(eq)}$ (Å^2)[a]
Tl	0.02294(9)	0.10991(8)	0.09900(8)	0.0228(2)
Te	−0.02574(12)	0.46798(11)	0.40160(12)	0.0086(2)
V	−0.2229(3)	0.2601(2)	0.7139(3)	0.0091(5)
O(1)	−0.2227(16)	0.1818(13)	0.5209(15)	0.016(2)
O(2)	0.1268(15)	0.6348(11)	0.4475(13)	0.011(2)
O(3)	−0.4347(16)	0.3262(13)	0.7411(14)	0.014(2)
O(4)	−0.1002(15)	0.4488(11)	0.6382(12)	0.010(2)
O(5)	−0.2536(15)	0.0774(12)	0.8472(14)	0.014(2)

[a] $U_{(eq)}$ is defined as one-third of the trace of the orthogonalized U_{ij} tensor.

Table 5. Selected Bond Distances (Å) for $TlTeVO_5$

	Bond distance
V−O(1)	1.666(12)
V−O(2)	2.172(10)
V−O(3)	1.669(12)
V−O(3)	2.250(12)
V−O(4)	1.971(10)
V−O(5)	1.926(11)
Te−O(2)	1.873(10)
Te−O(4)	1.947(10)
Te−O(4)	2.383(10)
Te−O(5)	1.926(11)
Tl−O(1)	3.005(12)
Tl−O(2)	2.759(10)
Tl−O(2)	2.835(11)
Tl−O(3)	2.798(11)
Tl−O(3)	2.888(11)
Tl−O(4)	3.414(11)
Tl−O(5)	2.847(11)
Tl−O(5)	3.057(11)

to $TlSeVO_5$, the structure of $TlTeVO_5$ consists of chains of corner-shared VO_6 octahedra that run along the *a*-axis. Similar to $TlSeVO_5$, in $TlTeVO_5$ inter- and intrachain connections are made through the TeO_4 polyhedra. Also similar to the reported selenite, in $TlTeVO_5$, TlO_8 polyhedra connect the VO_6 and TeO_4 groups resulting in a three-dimensional crystal structure (see Figure 2). With $TlTeVO_5$, the V^{5+}, Te^{4+}, and Tl^+ cations are in asymmetric coordination environments attributable to SOJT effects. The V^{5+} cations are in distorted octahedral environments, bonded to six oxygen atoms, with V−O bond distances ranging from 1.666(12) to 2.250(12) Å (see Table 5). The V^{5+} cation undergoes an out-of-center distortion attributable to SOJT effects that create bond asymmetries within the VO_6 octahedron. Two "short" (1.666(12) and 1.669(12) Å), two "normal" (1.926(11) and 1.971(10) Å), and two "long" (2.172(10) and 2.250(12) Å) V−O bonds are observed, resulting in a V^{5+} distortion toward an edge of the VO_6 octahedron (local C_2 direction). The Te^{4+} cations are in distorted square pyramidal environments, attributable to their lone-pair, bonded to four oxygen atoms, with Te−O bond distances ranging from 1.873(10) to 2.383(10) Å. The Tl^+ cations are also in asymmetric coordination environments, attributable to their lone-pair, bonded to eight oxygen atoms. The Tl−O bond distances range from 2.759(10) to 3.414(11) Å (see Table 5). In connectivity terms, the structure may be written as $[(VO_{4/2}O_{1/3}O)^{1.66-}(TeO_{2/2}O_{2/3})^{0.66+}]^-$ with charge balance maintained by the Tl^+ cation. The bond valence calculations[39,40] resulted in values of 0.96, 3.89, and 4.90 for Tl^+, Te^{4+}, and V^{5+} cations, respectively.

Infrared and Raman Spectroscopy. The infrared and Raman spectra of $TlSeVO_5$ and $TlTeVO_5$ revealed V−O, terminal V−O (V═O), V−O−V, M−O, and M−O−V (M = Se^{4+} or Te^{4+}) vibrations. The stretches, in the ranges 930−900, 900−700, and 700−780 cm^{-1}, can be attributed to terminal V−O (V═O), V−O, and V−O−V vibrations, respectively, whereas the stretches in the ranges 764−464 and 786−643 cm^{-1} can be attributed to Se−O and Te−O vibrations, respectively, in both IR and Raman spectra. The infrared and Raman vibrations and their assignments are listed in Table 6. The assignments are consistent with those previously reported.[27,41−44]

UV−Vis Diffuse Reflectance Spectroscopy. Both $TlSeVO_5$ and $TlTeVO_5$ are yellow. The UV−vis diffuse reflectance spectra indicate that the absorption energy for both compounds is approximately 2.2 eV. Absorption (*K*/*S*) data were calculated from the Kubelka−Munk function:[36]

$$F(R) = \frac{(1-R)^2}{2R} = \frac{K}{S}$$

with *R* representing the reflectance, *K* the absorption, and *S* the scattering. In a *K*/*S* versus *E* (eV) plot, extrapolating the linear part of the rising curve to zero provides the onset of absorption at 2.20 and 2.16 eV for $TlSeVO_5$ and $TlTeVO_5$, respectively. It is suggested that the electronic transition occurs between the filled highest energy orbitals, Tl 6s and 6p, and the lowest unoccupied orbitals, V 3d. The UV−vis diffuse reflectance spectra for the reported compounds have been deposited in the Supporting Information.

Thermal Analyses. The thermal behavior of $TlMVO_5$ (M = Se^{4+} or Te^{4+}) was investigated using thermogravimetric analysis (TGA). $TlSeVO_5$ and $TlTeVO_5$ decompose at 300 and 700 °C, respectively. The TGA curve for $TlSeVO_5$ reveals a one step decomposition from 300 to 500 °C attributable to the sublimation of one mole of SeO_2: calcd

(41) Frost, R. L.; Erickson, K. L.; Weier, M. L.; Carmody, O. *Spectrochim. Acta* **2005**, *61A*, 829.
(42) Sivakumar, T.; Ok, K. M.; Halasyamani, P. S. *Inorg. Chem.* **2006**, *45*, 3602.
(43) Ok, K. M.; Halasyamani, P. S. *Chem. Mater.* **2002**, *14*, 2360.
(44) Vaughey, J. T.; Harrison, W. T. A.; Dussack, L. L.; Jacobson, A. J. *Inorg. Chem.* **1994**, *33*, 4370.

Table 6. Infrared and Raman Data (cm^{-1}) for $TlMVO_5$ (M = Se^{4+} or Te^{4+})

$TlSeVO_5$					$TlTeVO_5$				
V=O	V−O	Se−O	V−O−V	Se−O−V	V=O	V−O	Te−O	V−O−V	Te−O−V
IR (cm^{-1})									
903	885	767	730	657	902	850	784	747	647
	808	649	708			829	715		
	799	537				807	671		
	606	522				614			
	581	464				513			
	492								
Raman (cm^{-1})									
911	897	764	775		927	894	785	766	638
904	885	756	745		903	855	710	740	
	832					844	643		
	798					802			
						436			
						404			

(exp) 26.78% (26.82%), resulting in the formation of $TlVO_3$.

$$TlSeVO_5 \xrightarrow[300-500\ ^\circ C]{\Delta} SeO_2\uparrow + TlVO_3$$

Powder XRD pattern of the calcined product of $TlSeVO_5$, at 600 °C for 12 h, confirms the formation of $TlVO_3$[45] (see Figure S10, Supporting Information). $TlTeVO_5$ melts at ~415 °C, and a single-step decomposition occurs, indicating volatilization, above 700 °C. The differential scanning calorimetric (DSC) analysis for $TlTeVO_5$ reveals a strong endothermic peak at 415 °C attributable to the melting of $TlTeVO_5$ (see Figure S11, Supporting Information). Powder XRD patterns of $TlSeVO_5$ heated at 230 °C in air for 12 h, and $TlTeVO_5$ heated at 400 °C for 10 min in air, reveal that $TlSeVO_5$ and $TlTeVO_5$ are stable in air up to 230 and 400 °C, respectively. The TGA and DSC curves for both of the materials are available in the Supporting Information.

Second Harmonic Generation. Because both $TlSeVO_5$ and $TlTeVO_5$ crystallize in noncentrosymmetric space group, $Pna2_1$, SHG measurements were carried out. Powder SHG measurements using 1064 nm radiation revealed that $TlSeVO_5$ and $TlTeVO_5$ have SHG efficiencies of approximately 40 × α-SiO_2. By sieving $TlSeVO_5$ and $TlTeVO_5$ into various particle sizes, ranging from 20 to 120 μm, and measuring the SHG as a function of particle size, we were able to determine the type 1 phase-matching capabilities of the materials (see Supporting Information). We determined both of the materials, $TlSeVO_5$ and $TlTeVO_5$, are non-phase-matchable, indicating the materials fall into the class C category of SHG materials as defined by Kurtz and Perry.[37] As previously shown, once the SHG efficiency has been measured and the phase-matching behavior determined, the average NLO susceptibility, $\langle d_{eff}\rangle_{exp}$, can be estimated.[13] For non-phase-matchable materials

$$\langle d_{eff}\rangle_{exp} = \{0.3048[I^{2\omega}(TlSeVO_5 \text{ or } TlTeVO_5)/I^{2\omega}(SiO_2)]\}^{1/2}$$

where $I^{2\omega}(SiO_2) = 1.0$ (the SHG efficiency of α-$SiO_2 = 1.0$). Thus, $\langle d_{eff}\rangle_{exp}$ for $TlSeVO_5$ and $TlTeVO_5$ is approximately 3.5 pm V^{-1}, respectively.

Piezoelectric Measurements. Attributable to the low decomposition temperatures of the materials, it was not possible to press or sinter $TlSeVO_5$ or $TlTeVO_5$ into appropriately dense pellets for our converse piezoelectric measurements.

Ferroelectric Measurements. Although $TlSeVO_5$ and $TlTeVO_5$ are polar, they are not ferroelectric; that is, their dipole moment (polarization) cannot be reversed in the presence of an external electric field. Polarization versus electric field data for $TlSeVO_5$ and $TlTeVO_5$ have been deposited in the Supporting Information.

Pyroelectric Measurements. Polarization measurements, at room temperature, utilizing an electric field of 20 kV/cm, indicated a maximum polarization of 0.16 and 0.13 μC/cm^2 for $TlSeVO_5$ and $TlTeVO_5$, respectively. The maximum polarization for both materials decreases with increasing temperature. To determine the total pyroelectric coefficient, *p*, the change in polarization as a function of temperature was measured. The total pyroelectric coefficients, $p = (dP_s/dT)$, where P_s is the spontaneous polarization and *T* is the temperature, for $TlSeVO_5$ and $TlTeVO_5$ are −2.9 and −1.9 μC/m^2·K. The magnitudes of the pyroelectric coefficients for both materials are consistent with other known non-ferroelectric pyroelectrics such as ZnO (−9.4 μC/m^2·K) and tourmaline (−4.0 μC/m^2·K).[46]

Discussion

Both $TlSeVO_5$ and $TlTeVO_5$ crystallize in the noncentrosymmetric polar space group $Pna2_1$, with very similar unit cells. For $TlSeVO_5$ ($TlTeVO_5$), $a = 7.1639(15)$ Å (7.319(3) Å), $b = 8.6630(19)$ Å (8.749(4) Å), $c = 7.8946(17)$ Å (7.868(3) Å), and $V = 489.95(18)$ $Å^3$ (503.8(4) $Å^3$). The materials, however, are not iso-structural. If we examine Figures 1 and 2, we notice that the Se^{4+} cation is three-coordinate, whereas the Te^{4+} cation is four-coordinate, respectively. The decreased coordination, three versus four, as well as size, 0.50 versus 0.66 Å, for Se^{4+} as compared to Te^{4+}, results in a slightly smaller unit cell volume for $TlSeVO_5$ as compared to $TlTeVO_5$. As stated earlier, all of the cations are in asymmetric coordination environments attributable to SOJT effects. With Se^{4+}, Te^{4+}, and Tl^+, a lone-pair is observed that produces "gaps" in the structure running down the *a*-axis (see Figures 1 and 2). For the V^{5+} cation, the SOJT effects result in an intra-octahedral displacement toward an edge (local C_2 direction), creating two

(45) Ganne, M.; Piffard, Y.; Tournoux, M. *Can. J. Chem.* **1974**, *52*, 3539.

(46) Lang, S. B. *Phys. Today* **2005**, *58*, 31.

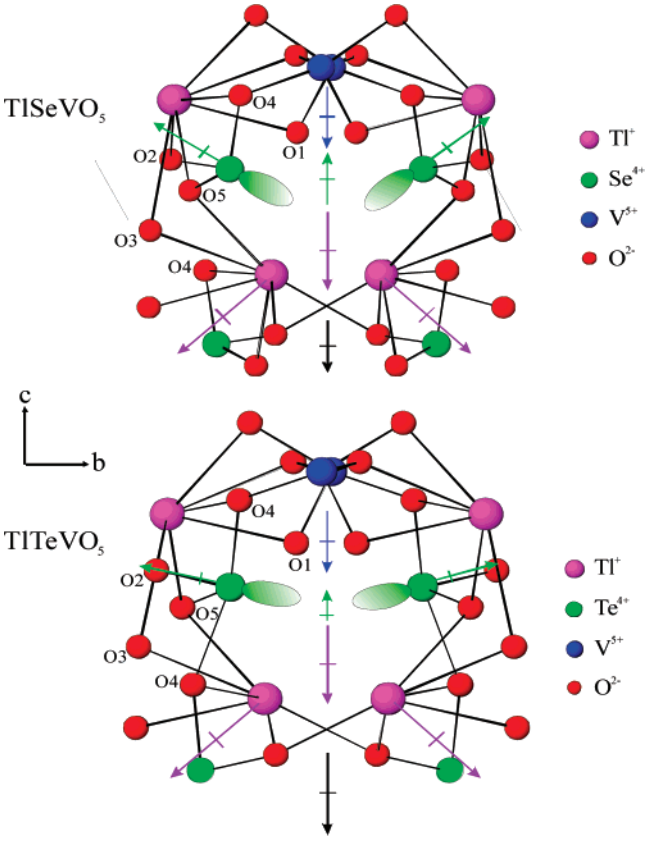

Figure 3. Ball-and-stick diagram showing the local moments in $TlSeVO_5$ (top) and $TlTeVO_5$ (bottom). The magnitude of the local moments and lone-pairs are shown schematically. As seen there is slightly more cancellation of the moments for $TlSeVO_5$ as compared to $TlTeVO_5$.

"short", two "normal", and two "long" V−O bonds. We have previously shown that this C_2-type of distortion is relatively common for V^{5+} cations.[25]

We have also determined the magnitude of the cationic distortions by calculating the local dipole moments, as well as by using continuous symmetry measures.[47,48] In calculating the dipole moments for the V^{5+}, Se^{4+}, Te^{4+}, and Tl^{+} cations, we used a methodology described earlier[49,50] that has been expanded to include lone-pair cations.[51] With the lone-pair polyhedra, the lone-pair is given a charge of −2 and is localized 1.22, 1.25, and 0.69 Å from the Se^{4+}, Te^{4+}, and Tl^{+} cations, respectively. The cation−lone-pair distance is based upon earlier work by Galy and Meunier.[52] The dipole moment calculations for $TlSeVO_5$ ($TlTeVO_5$) resulted in values of 8.93D (9.60D) for V^{5+}, 8.00D for Se^{4+} (10.21D for Te^{4+}), and 1.30D (1.63D) for Tl^{+}. The magnitudes are consistent with previously reported values.[51] In addition to dipole moment calculations, we used a continuous symmetry measures methodology to calculate the magnitude of the V^{5+} distortion.[47,48] Utilizing the SHAPE program,[53] we calculated an intra-octahedral distortion of 0.138 and 0.140 $Å^2$ for the V^{5+} cation in $TlSeVO_5$ and $TlTeVO_5$, respectively. These values are slightly less than the average value of 0.145 $Å^2$ reported earlier.[25]

All of the cation distortions, both magnitude and direction, influence the observed physical properties. With the direction of the cationic distortions in $TlSeVO_5$, we notice that the V^{5+} cations are directed toward the [00−1]. Each Se^{4+} cation has its dipole moment pointed toward the [011] and [0−11], resulting in a net moment pointing along the [001]. Finally, each Tl^{+} cation has its dipole moment directed toward the [0−1−1] and [01−1], resulting in a net moment pointing along the [00−1]. Thus, if we add all of the dipole moment directions, V^{5+} [00−1], Se^{4+} [001], and Tl^{+} [00−1], we have a net moment for $TlSeVO_5$ in the [00−1]. Similar cationic distortions, with respect to direction, are observed in $TlTeVO_5$, with the dipole moments from the V^{5+} and Tl^{+} cations pointing toward the [00−1], and the Te^{4+} pointing toward the [001], resulting in a net moment toward the [00−1]. One difference in the direction of the local dipole moment is observed with the Se^{4+} and Te^{4+} cations. Although both cations have their moments pointed in the very approximate [0±1−1], the majority of the Te^{4+} moment is directed along the [0±10] (see Figure 3). Thus, any contribution of the total moment, in $TlTeVO_5$, from Te^{4+} is negligible. With respect to the measured acentric physical properties, the magnitudes are similar for both reported materials. This is perhaps somewhat surprising given that there is less cancellation of the local dipole moments in $TlTeVO_5$ as compared to $TlSeVO_5$. It is likely, however, that the amount of cancellation is not as different as estimated, which results in similar magnitudes for the acentric physical properties.

Acknowledgment. We thank the Robert A. Welch Foundation and the Texas Center for Superconductivity (University of Houston) for support. This work was supported by the NSF through DMR-0092054. We also acknowledge Vicky Mody and Prof. Roman Czernuszewicz, and Timothy Fulghum and Prof. Rigoberto Advincula for assistance in obtaining the Raman spectra and DSC data.

Supporting Information Available: X-ray crystallographic information for $TlSeVO_5$ and $TlTeVO_5$ (TXT) and ORTEP diagrams, experimental and calculated powder XRD patterns, IR spectra, Raman spectra, UV−vis diffuse reflectance curves, thermogravimetric and differential scanning calorimetric analyses curves, SHG phase-matching curves, polarization and pyroelectric data, and dipole moment calculations for two reported materials (PDF, Excel). This material is available free of charge via the Internet at http://pubs.acs.org.

CM071188P

(47) Zabrodsky, H.; Peleg, S.; Avnir, D. *J. Am. Chem. Soc.* **1992**, *114*, 7843.
(48) Alvarez, S.; Alemany, P.; Casanova, D.; Cirera, J.; Llunell, M.; Avnir, D. *Coord. Chem. Rev.* **2005**, *249*, 1693.
(49) Maggard, P. A.; Nault, T. S.; Stern, C. L.; Poeppelmeier, K. R. *J. Solid State Chem.* **2003**, *175*, 25.
(50) Izumi, H. K.; Kirsch, J. E.; Stern, C. L.; Poeppelmeier, K. R. *Inorg. Chem.* **2005**, *44*, 884.
(51) Ok, K. M.; Halasyamani, P. S. *Inorg. Chem.* **2005**, *44*, 3919.
(52) Galy, J.; Meunier, G. *J. Solid State Chem.* **1975**, *13*, 142.
(53) Llunell, M.; Casanova, D.; Cirera, J.; Bofill, J. M.; Alemany, P.; Alvarez, S.; Pinsky, M.; Avnir, D. *SHAPE*, 1.1b ed.; University of Barcelona: Barcelona, Spain, 2004.